INVESTIGATION OF SPACE-CHARGE-LIMITED CONDUCTION MECHANISMS IN FE_3O_4-γ-FE_2O_3 BASED ON SIO_2/N-TYPE SI SUBSTRATE

NIK NADIA AINA BINTI NIK ZUMAIHAN

FACULTY OF ENGINEERING
UNIVERSITY OF MALAYA
KUALA LUMPUR

2020

INVESTIGATION OF SPACE-CHARGE-LIMITED CONDUCTION MECHANISMS IN FE_3O_4-γ-FE_2O_3 BASED ON SIO_2/N-TYPE SI SUBSTRATE

NIK NADIA AINA BINTI NIK ZUMAIHAN

DISSERTATION SUBMITTED IN PARTIAL FULFILMENT OF THE REQUIREMENTS FOR THE DEGREE OF MASTER IN MECHANICAL ENGINEERING

FACULTY OF ENGINEERING
UNIVERSITY OF MALAYA
KUALA LUMPUR

2020

UNIVERSITY OF MALAYA

ORIGINAL LITERARY WORK DECLARATION

Name of Candidate: **NIK NADIA AINA BINTI NIK ZUMAIHAN**

Matric No: **17199131**

Name of Degree: **MASTER IN MECHANICAL ENGINEERING**

Title of Project Paper/Research Report/Dissertation/Thesis ("this Work"):

INVESTIGATION OF SPACE-CHARGE-LIMITED CONDUCTION MECHANISMS IN FE_3O_4-γ-FE_2O_3 BASED ON SiO_2/N-TYPE SI SUBSTRATE

Field of Study: **ADVANCED MATERIALS/THIN FILM GATE OXIDE**

I do solemnly and sincerely declare that:

(1) I am the sole author/writer of this Work;
(2) This Work is original;
(3) Any use of any work in which copyright exists was done by way of fair dealing and for permitted purposes and any excerpt or extract from, or reference to or reproduction of any copyright work has been disclosed expressly and sufficiently and the title of the Work and its authorship have been acknowledged in this Work;
(4) I do not have any actual knowledge nor do I ought reasonably to know that the making of this work constitutes an infringement of any copyright work;
(5) I hereby assign all and every rights in the copyright to this Work to the University of Malaya ("UM"), who henceforth shall be owner of the copyright in this Work and that any reproduction or use in any form or by any means whatsoever is prohibited without the written consent of UM having been first had and obtained;
(6) I am fully aware that if in the course of making this Work, I have infringed any copyright whether intentionally or otherwise, I may be subject to legal action or any other action as may be determined by UM.

Candidate's Signature Date:

Subscribed and solemnly declared before,

Witness's Signature Date:

Name:

Designation:

INVESTIGATION OF SPACE-CHARGE-LIMITED CONDUCTION MECHANISMS IN FE_3O_4-Γ-FE_2O_3 BASED ON SIO_2/N-TYPE SI SUBSTRATE

ABSTRACT

In this work, thin films of functionalized Fe_3O_4-γ-Fe_2O_3 NPs deposited on n-type Si substrate was formed by self-assembly. The co-precipitation method was involved to synthesis the bare iron oxide NPs and the particles were altered to optimum pH 12 by using NH_4OH. Iron oxide NPs were then undergone modification process with addition of 0.4 g oleic acid and 1.63 mmol functionalization 4-pentynoic acid. For electrical characterization of self-assembled 4-pentynoic acid functionalized Fe_3O_4-γ-Fe_2O_3 NPs on SiO_2/n-Si substrate, the charge conduction mechanisms were quantitatively investigated and analyzed through the oxides for different heat treatment temperatures (70-300^oC). In this study, the Ohm's Law and PF emission were intensively investigated to identify the leakage current density of the tested materials using SigmaPlot based on J-E plot data provided. At the lower electric field, the leakage current due to Ohm's law is the major sources contributing to oxide breakdown at the electrical breakdown field, E_B level. On the other hand, the PF emission was identified and analyzed at the higher electric field before the electric breakdown occur. The highest E_B was showed by the heat-treated sample of 150^oC with values of 2.58×10^{-3}MV/cm approximately at 10^{-3} A/cm^2 and it obeys the Ohm's law as the slope is near to 1. For dynamic dielectric constant (k_r), the sample heated at 200^oC showed promising value compared to other temperatures and acquired *k*-value (7.99) higher than commercial native oxide, SiO_2 (3.8-3.9). However, its E_B is considered low which limits its performance electrically. Besides, the heat-treated sample of 150^oC demonstrated the best outcomes as the leakage current is low (10^{-3}A/cm^2), high E_B (2.58×10^{-3}MV/cm) and has k_r near to *k* of SiO_2 (3.85).

Keywords: Thin film, iron oxide NPs, gate dielectric, charge conduction mechanism

KAJIAN TERHADAP MEKANISME KONDUKSI RUANG CAS TERHAD TERHADAP FE_3O_4-Γ-FE_2O_3 DI ATAS SIO_2/SI SUBSTRAT JENIS-N

ABSTRAK

Dalam kajian ini, filem nipis magnetit-maghemite berfungsi (Fe3O4-γ-Fe2O3) nanopartikel (NP) yang disimpan pada substrat silikon (Si) jenis-n dibentuk dari pembentukan sendiri. Kaedah pemendakan-bersama terlibat untuk mensintesis NP besi oksida terdedah dan zarah-zarah diubah menjadi pH 12 optimum dengan menggunakan NH4OH. NP besi oksida kemudian menjalani proses pengubahsuaian permukaan dengan penambahan 0.4 g asid oleik dan 1.63 mmol asid 4-pentynoik. Untuk pencirian elektrik keatas sampel yang dihasilkan, mekanisme konduksi cas melalui lapisan oksida disiasat dan dianalisis secara kuantitatif untuk suhu haba yang berbeza (70-300^oC). Graf J-E telah telah dilengkapi dengan kemasukan mekanisme pengaliran caj yang berbeza. Dalam kajian ini, Hukum Ohm dan pelepasan PF disiasat secara intensif untuk mengenal pasti ketumpatan arus kebocoran bahan yang diuji. Di medan elektrik yang lebih rendah, arus kebocoran yang disebabkan oleh Hukum Ohm adalah sumber utama yang menyumbang kepada kerosakan oksida di medan pemecahan elektrik, E_B. Selain itu, pelepasan PF dikenal pasti dan dianalisis di medan elektrik yang lebih tinggi. E_B tertinggi ditunjukkan oleh sampel dengan suhu 150^oC dengan nilai 2.58 × 10-3 MV/cm dengan kebocoran arus lebih kurang 10^{-3} A/cm^2 dan ia mematuhi Hukum Ohm kerana cerun mendekati 1. Untuk pemalar dielektrik dinamik (k_r), sampel yang dipanaskan pada suhu 200^oC menunjukkan nilai yang menjanjikan dibandingkan dengan suhu lain dan mempunyai nilai *k* (7.99) lebih tinggi daripada oksida asli komersial, SiO_2 (3.8-3.9). Walau bagaimanapun, E_B pada suhu 200^oC dianggap rendah dimana menghadkan prestasinya secara elektrikal. Selain itu, sampel bahan dengan suhu 150^oC menunjukkan hasil terbaik kerana arus kebocoran

rendah (10^{-3} A/cm2), E_B tinggi (2.58×10^{-3} MV/cm) dan mempunyai k_r mendekati k SiO2 (3.85).

Kata kunci: Filem nipis, nanopartikel besi oksida, Pintu dielektrik, Mekanisme konduksi cas

ACKNOWLEDGEMENTS

First and foremost, I would like to praise the Allah the Almighty for His grace and faithfulness by giving me strength throughout this research project. Without His guidance, I am sure I will not be strong and brave enough to face the difficulties along the way and able to complete it.

My deepest appreciation to my supervisor, Assoc. Prof. Ir. Dr. Wong Yew Hoong for his generous support, guidance and gives me a lot of experiences while conducting my research project. Special thanks also go to all my friends, Vanessa Lusus, Nur Hasdyanna binti Hasnurashid and Nicklaane Krishnamoorthy, academic and administrative staffs of Faculty of Engineering for their assistances and support.

Lastly, I wish to thank my family for their endless support, helps and encouragement in completing this research project. Thanks to all that being a part of this exciting and memorable journey of my life.

TABLE OF CONTENTS

LIST OF FIGURES

LIST OF TABLES

LIST OF SYMBOLS AND ABBREVIATIONS

IC	:	Integrated circuit
CMOS	:	Complementary metal-oxide-semiconductor
MOSFET	:	Metal Oxide Semiconductor Field Effect Transistor
Si	:	Silicon
SiO_2	:	Silicon Dioxide
k	:	Dielectric constant
NPs	:	Nanoparticle
γ-Fe_2O_3	:	Maghemite
Fe_3O_4	:	Magnetite
C_{ox}	:	Oxide capacitance
κ_{ox}	:	Oxide dielectric constant
ε_0	:	Permittivity of free space
A_{ox}	:	Oxide area
E_g	:	Band gap electric field
Al_2O_3	:	Aluminium oxide
TiO_2	:	Titanium oxide
Ta_2O_5	:	Tantalum pentoxide
ZrO_2	:	Zirconium oxide
HfO_2	:	Hafnium oxide
Y_2O_3	:	Yttrium oxide
Fe_2O_3	:	Iron oxide
SiN_4	:	Silicon nitrides
α-Fe_2O_3	:	Hematite
MRI	:	Magnetic resonance imaging

NaOH	:	Sodium hydroxide
NH_4OH	:	Ammonium hydroxide
PVD	:	Physical vapour deposition
CVD	:	Chemical vapour deposition
RF	:	Radio frequency
PLD	:	Pulse laser deposition
EOT	:	Equivalent oxide thickness
MOCVD	:	Metal organic chemical vapour deposition
ALD	:	Atomic layer deposition
SAM	:	Self-assembly monolayers
OFET	:	Organic field-effect transistor
Von	:	Crossover voltage
PF	:	Poole-Frenkel
V_g	:	Gate voltage
V_{fb}	:	Flat band voltage
t_{ox}	:	Oxide thickness
q	:	Electronic charge
n_o	:	Concentration of charge carriers in thermal equilibrium
N_c	:	Density of states in the conduction band
$\emptyset_t$	:	Trap energy level in the oxide
k_r	:	Dynamic dielectric constant
T	:	Oxidation temperature
TFL	:	Trap-filled limit
SCLC	:	Space-charge-limited-conduction
PF	:	Poole-Frenkel

LIST OF APPENDICES

CHAPTER 1: INTRODUCTION

1.1 Background of Study

In this era of advanced technology, semiconductor devices are very important in human life to carry out their daily activities. They require excellent characteristic such as nano-scale size, high speed, low cost, high circuit density and low power consumption due to rapid development of semiconductor industry (Constantinescu, Ion, Galca, & Dinescu, 2012; Cui & Lieber, 2001; S. Kim et al., 2012; Liao et al., 2010). These aspects are very compulsory when it comes to design nanostructure materials of the medical devices with outstanding performances (Ar, S, M, Sss, & Sm, 2017).

Silicon (Si) material was once widely used in semiconductor industry for decades because of the capacity to form in large energy band gap, no structure defect of large single crystal, very low and controlled doping level and has ability to grow a native oxide (SiO_2). Silicon oxide (SiO_2) layer has been used as primary gate oxide on Si due to its excellent insulator properties. However, the continual miniaturization of SiO_2 gate dielectric thickness is restricted as it leads to a gate leakage current because of the high electrons tunnels at direct conditions. (Wong & Cheong, 2011, 2013) and low reliability against electrical breakdown (Goh, Haseeb, & Wong, 2016; J. Robertson, 2004). This gate leakage current increases the power dissipation and reduces IC stability and device performance (Sayed & Atef, 2005). Thus, there are numerous researches have been done to overcome the high leakage current issues by selecting the various types of materials instead of further downscaled of the gate oxide (Brassard, Sarkar, El Khakani, & Ouellet, 2004; Esro, Vourlias, Somerton, Milne, & Adamopoulos, 2015; Jeliazova, Kayser, Mildner, Hassel, & Diesing, 2006; Kamata, Kamimuta, Ino, & Nishiyama, 2005).

1.2 Problem statement

In recent year, the researchers have been widely studied of the magnetic nanoparticles (Ar et al., 2017; Rahdar, Taboada, Aliahmad, Hajinezhad, & Sadeghfar, 2018; Vangijzegem, Stanicki, & Laurent, 2019). In magnetic nanoparticles, iron oxide nanoparticles (NPs) are among the outstanding materials as it has good bio-safety, high magnetic susceptibility and high saturation magnetization, controllable characteristic and easy available than other NPs (Gupta & Gupta, 2005; Rahdar et al., 2018). In biomedical and clinical applications, maghemite (γ-Fe_2O_3) gives promising magnetic characteristics in magnetic resonance imaging, drug delivery, recording, cell targeting and memory devices (Ar et al., 2017; Gubin, Koksharov, Khomutov, & Yurkov, 2005; Y. Zhang, Kohler, & Zhang, 2002; Zhou et al., 2015). γ-Fe_2O_3 also known to have unique properties in its nanometer size. But, there are limitations of γ-Fe_2O_3 where they have tendency to agglomerate into micron size which then reducing their surface energy (Gupta & Gupta, 2005). As a result, a lot of studies has been done to solve the setbacks of agglomeration occurred in γ-Fe_2O_3 NPs (Gupta & Gupta, 2005; Rahdar et al., 2018; Y. Zhang et al., 2002).

One of the methods to overcome these setbacks are by introducing surfactant (attaching any compatible functional groups) to the γ-Fe_2O_3 NPs. In this study, surface modification of γ-Fe_2O_3 with oleic acid is carried out in order to abate the agglomeration (Shete, Patil, Tiwale, & Pawar, 2015). Moreover, ex-situ modifications with surfactants (oleic acid and 4-pentynoic acid) also were optimized in this study together with enhanced stability at pH 12 to obtain the best properties of γ-Fe_2O_3 NPs. To provide good electrical properties to the biomedical devices, the leakage characteristics thoroughly studied based on the analysing of charge conduction mechanisms for each of the oxidation temperature (70, 150, 200 and 300^{o}C). Various types of charge conduction mechanisms

such as space-charge limited current (SCLC), Schottky emission (SE), Poole-Frenkel (PF) emission and Fowler-Nordheim (FN) tunneling have been studied previously but limited (Baharuddin, Ang, & Wong, 2017; Wong & Cheong, 2011). Thus, this research aims to study and understand charge conduction mechanisms of SCLC (Ohm's Law) and PF emission by considering the leakage current density at lower and higher applied voltage until reached the electric breakdown.

1.3 Research objectives

There are objectives of this study:

1. To study Ohm's Law behaviour in Fe_3O_4-γ-Fe_2O_3/SiO_2/n-type Si system
2. To investigate the Poole-Frenkel conduction mechanisms in Fe_3O_4-γ-Fe_2O_3/SiO_2/n-type Si system

1.4 Scope of study

In this study, there are three major division in scope of study:

Stage 1

Synthesis of Fe_3O_4-γ-Fe_2O_3 NPs by co-precipitation method. The effect of 0.4 g/g oleic acid and 4-pentynoic acid added to iron oxide will be investigated.

Stage 2

Fabrication of Fe_3O_4-γ-Fe_2O_3 FNPs on SiO_2/n-type Si substrate by self-assembly deposition method. SiO_2 was deposited on the Si substrate with varied oxidation temperature (70, 150, 200 and 300°C).

Stage 3

The effect on different temperature-influential self-assembly of Fe_3O_4-γ-Fe2O3/SiO2/n-type Si substrate on the electrical characteristics of the fabricated MOS will be analysed from the I-V measurements.

1.5 Outline overview

The overall outline of this research project is set out according to the structure below to give a wide idea of the conducted research work. Chapter 1 is basically a general review of the background, current issues and limitations in technologies of semiconductor. Besides, the advantages and disadvantages of γ-Fe_2O_3 NPs were also briefly mentioned along with objectives and scope of the research study. Then, Chapter 2 involved of literature review which begins with introduction of MOSFET, limitation of existing SiO_2 gate dielectric, common materials used as gate dielectric, development and surface modification of iron oxide NPs and common deposition methods used in iron oxide NPs Chapter 3 is the methodology of the research work described the electrical characterization analysis procedures of self-assembly of functionalized Fe_3O_4-γ-Fe_2O_3 NPs on SiO_2/n-type Si substrate based on the charge conduction mechanisms of Ohm's Law and Poole-Frenkel emission. The results and discussion of the self-assembled

samples are presented in Chapter 4. In Chapter 5, the conclusion and some future recommendations of the research work is included.

CHAPTER 2: LITERATURE REVIEW

2.1 Introduction

The continuous development of CMOS integrated circuit technologies is now dominating with high specifications of electronic devices such as transistors and capacitors. Based on Moore's law, the number of components on IC would double every two to three years and his prediction is proven by the high development of semiconductor industry (M. T. Bohr & Young, 2017; John Robertson & Wallace, 2015; Smit, van der Tol, & Hill, 2012) . Downscaled the dimension of the components in devices is one of the achievements in semiconductor industry as it provides low power consumption at the high level of devices speed. Generally, the MOSFET scaling can be sorted into three purposes (M. Bohr, 2009; Chaudhry & Roy, 2010; Ng & Lynch, 1987):

i. More transistors accommodated on a single chip, thus multi tasks can be performed with low cost of chip production,
ii. Intended for downscale the geometry of IC to increase circuit density that need smaller length and width of channel and
iii. Accelerate the charging and discharging of capacitance and at the same time increase the transistor current.

However, further scaling down of the components has reached the limit due to drawbacks which are uncontrolled leakage current and unfavorable performance of devices (Goh et al., 2016; Williams, 2017). Hence, the limitations of current Si substrate and SiO_2 gate dielectric will be reviewed. The materials to add on the Si substrate and SiO_2 are also will be described including their general properties and previous studies.

2.2 Limitation of SiO_2 gate dielectric

Si substrate and its native oxide, SiO_2 has been used for years in semiconductor industry as they offered high thermodynamic stability and outstanding electrical isolation properties (Constantinescu et al., 2012; Wilk, Wallace, & Anthony, 2001). Besides, the SiO_2 layers also have an excellent interface with Si substrate, thereby exhibits high performance in MOS device properties (Wilk et al., 2001).

The continuous shrinkage of Si-based MOS devices has attributed to the improvement in density and performance of transistors in an IC chip (Chiu & Lai, 2010; Wong & Cheong, 2011). However, further downscaling below 3 nm of SiO_2 gate dielectric thickness would impose several problems, including high gate leakage current mainly caused by the excessive gate tunneling in SiO_2, resulting in excessive power dissipation and deterioration of device functionality (Chiu & Lai, 2010; Constantinescu et al., 2012; Salmani-Jelodar et al., 2016). For SiO_2 at 1 V gate bias, the current density in significantly increased from 10^{-6} A/cm^2 to 10 A/cm^2 when the gate dielectric reduced in thickness of 3 nm to 1 nm as shown in Figure 2.1.

Hence, the alternative way to overcome direct tunneling occurs in current oxide layer is by introducing lower thickness of new high-k oxide without reducing its capacitance to SiO_2. The implementation of organic oxide materials into gate stacks can be well interpreted using Equation 2.1.

$$C_{ox} = \frac{\kappa_{ox}\varepsilon_0 A_{ox}}{t_{ox}} \tag{2.1}$$

where C_{ox} is the oxide capacitance, κ_{ox} is the oxide dielectric constant, ε_0 is the permittivity of free space (8.85×10^{-2} pC/V.m), A_{ox} is the oxide area and t_{ox} is the oxide thickness (Wong & Cheong, 2010).

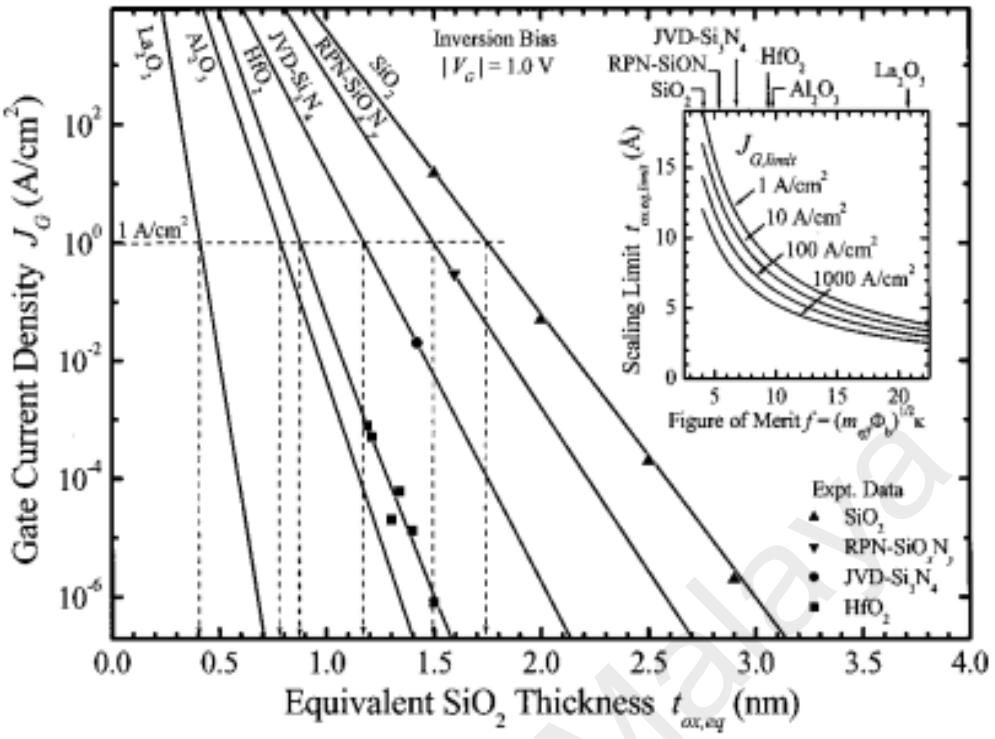

Figure 2.1: Gate current density, J_g at different oxide thickness

(Yeo, King, & Hu, 2002)

2.3 Common material used as gate dielectric

There are several common materials are being investigated. However, there are some issues and limitations when all of the materials are applied to SiO_2. They have thermal instability and low interface quality with the Si substrate which mainly caused by high defect densities (Misra, Iwai, & Wong, 2005; J. Robertson, 2004; John Robertson & Wallace, 2015). Table 2.2 shows that the further explanation of the issues arisen from the high-*k*/Si system.

Table 2.1: Summary of common metal oxides

(Heng, 2017)

Materials	*k*	Band gap (eV)	Band offset with Si (eV)	Findings
Al_2O_3	9	8.8	2.8	High thermal stability, large interfacial trap, large fixed charge, large flatband voltage shift
TiO_2	80	3.5	0	No conduction offsets, low thermodynamic stability, low temperatures limit in crystallization
Ta_2O_5	22	4.4	0.35	Low thermodynamic stability, low conduction offset
ZrO_2	25	5.8	1.5	Formation of interfacial layer with high interface density, large flatband voltage shift
HfO_2	25	5.8	1.4	Formation of interfacial layer with high interface density, large flatband voltage shift, high trapped charges due to high oxygen concentration
Y_2O_3	15	6	2.3	Large conduction offset, low crystallization temperatures, high thermal stability, low lattice mismatch, higher interface density than SiO_2

2.4 Development of iron oxide NPs on Si substrate

2.4.1 Iron oxide NPs

In recent years, iron oxide nanoparticles (NPs) are widely employed in various applications, such as data storage devices, magnetic resonance imaging (MRI) contrast agents, magnetic fluids, supercapacitors, hyperthermia treatment, cell targeting, gas sensors, catalyst support and drug delivery (Akbarzadeh, Samiei, & Davaran, 2012; Ar et al., 2017; Guardia, Labarta, & Batlle, 2011; Jing et al., 2012; Lu, Salabas, & Schuth, 2007; Mahmoudi, Sant, Wang, Laurent, & Sen, 2011; Riaz, Bashir, & Naseem, 2014). The iron oxide NPs are one of the promising materials among magnetic NPs due to its low cost, low toxicity, high magnetic susceptibility, and environment friendly (Filippousi et al., 2014). The derivatives of iron oxide NPs include magnetite (Fe_3O_4), maghemite (γ-Fe_2O_3), and hematite (α-Fe_2O_3) where every phase of iron oxide NPs possesses varied characteristics depending on its application. Thus, it is essential to synthesis the iron oxide NPs to optimum particle size, morphology, particle geometry and size distribution when in the nanomaterials' areas (Darroudi, Hakimi, Goodarzi, & Kazemi Oskuee, 2014; Rashdan, Bououdina, & Al-Saie, 2013). Besides, the chemical stabilization of NPs in different states also is one of the key reasons for the success of NPs to the aforementioned areas and work optimum under the critical range size approximately 10-20 nm (Lu et al., 2007; Woo et al., 2004).

2.4.2 Properties of iron oxide NPs

Iron oxide nanoparticles (NPs) possess unique features compared to equivalent larger-scale materials. However, the iron oxide NPs have very high tendency of aggregation and adhesion as they possess differ surface interaction and structures than the sub-micron sized particles (X.-M. Li, Xu, Liu, & He, 2011; Soares et al., 2014). Thus, the development of some techniques to slow down the aggregation phenomena are highly recommended in NPs materials so that they can be implemented well in the industrial applications.

Among the iron oxides stated in Table2.3, magnetite (Fe_3O_4) is highly favorable among researchers because it has a superparamagnetic behavior at room temperature, non-toxicity, high compatibility and high saturation field. This characteristics makes it suits to be implement in many applications which mostly in biomedical and biotechnology fields (Mahmoudi et al., 2011). However, Fe_3O_4 is found not stable during oxidation process at high temperature and has a tendency to transform to maghemite (γ-Fe_2O_3) or hematite (α-Fe_2O_3). Nonetheless, the α-Fe_2O_3 can be formed back to Fe_3O_4 through hydrogen reduction process (Lu et al., 2007).

Other than that, Fe_3O_4 is a promising candidate to be implemented in spin electronic applications due to its half metallic properties that provides strong tendency to form interaction between electrons and atoms (polarons) in solid material below Curie temperature (*Tc*=860 K) and has small activation energy (Shete et al., 2015). However, the mutual spin-coupling forces are eliminated if temperature exceeds Tc. Last but not least, Fe_3O_4 has good electrical conductivity due to the Fe^{2+} and Fe^{3+} ions located randomly while maintaining its neutral charge.

2.4.3 Method used to synthesis iron oxide NPs

The synthesis of iron oxide NPs in nano range has been challenging among researchers in order to make them suitable to be used in various applications' field. Based on previous report, the properties of iron oxide NPs are depending on experimental conditions during preparation method such as pH, solvent, temperature, chemical routes, gas atmosphere, type of precursors and ex-situ treatment (Rashdan et al., 2013). All of the stated parameters are essential in producing the optimum particle size, magnetization and size of distribution of the NPs. Thus, it is very important to optimize all of the parameters in order to obtain the outstanding properties of the NPs.

In recent years, various synthesizing methods of iron oxide NPs have been reported in the literature. The proper selection of methods needs to be taken into account to retain the good quality of products' size, structure and morphology (Pang, Lim, Ong, & Chong, 2016). The methods that commonly used to synthesis iron oxide NPs are co-precipitation, hydrothermal, solvothermal, thermal decomposition and microemulsion process (Pang et al., 2016). Among all of those methods, co-precipitation is highest investigated by many researchers due to its best and simplest process among other methods (Y. Li et al., 2016).

The co-precipitation method involved the reaction between two ferrofluids, Fe^{2+} and Fe^{3+} salt solution with the addition of sodium hydroxide (NaOH) or ammonium hydroxide (NH_4OH) as a precipitating agent (Jing et al., 2012; Rashdan et al., 2013). The molar ratio that commonly used in the co-precipitation method for the mentioned ferrofluids was 1:2 (Pang et al., 2016). In addition, the composition, size and shapes of the iron oxide NPs are influenced by the type of salt solutions used, reaction temperature, pH value, molar ratio, introduction of surfactants, types of stabilizing agent and other

reaction parameters (Gupta & Gupta, 2005; X.-M. Li et al., 2011). However, the co-precipitation method has its own shortcomings. These include the difficulty to avoid the particle nucleation throughout the process and the formed particles have a weak magnetic response (Pang et al., 2016). As results, synthesized particles are relatively large, irregular morphology, wide-ranging distribution and poor crystallinity (Jing et al., 2012). Thus, there are very important to apply suitable modification on the particles to give some improvement in their features to suit their specific applications.

2.5 Surface modification of iron oxide NPs

As mentioned earlier, iron oxide NPs have extremely high tendency of aggregation and tend to be unstable due to large surface-to-volume ratio (Filippousi et al., 2014; Mahdavi et al., 2013). Then, these particles are prone to agglomerate and reduce the surface energy. However, the drawback can be overcome by applying surfactants as a coating to the iron oxide NPs intended to introduce repulsive force (steric and electrostatic repulsion) between the NPs (Soares et al., 2015). Thus, the surface modification of iron oxide NPs would improve their solubility in solvent, particle stabilization, particle dispersion and the most important is to reduce agglomeration (Khalil, Yu, Liu, & Lee, 2014; Mahdavi et al., 2013; Zhu et al., 2018).

Oleic acid is a fatty acid that has commonly used as coating agent in surface modification of iron oxide for their high affinity to the surface of iron oxide compared to other surfactants. In these methods, oleic acid is coordinating its non-polar hydrocarbon tail and polar carboxylic end groups on iron oxide NPs surface. Hence, the hydrocarbon tails of the oleic acid were pointed outwards from the surface of the synthesized iron

oxide NPs (Lee & Harris, 2006). Figure 2.2 illustrated the reaction of oleic acid with magnetic nanoparticles.

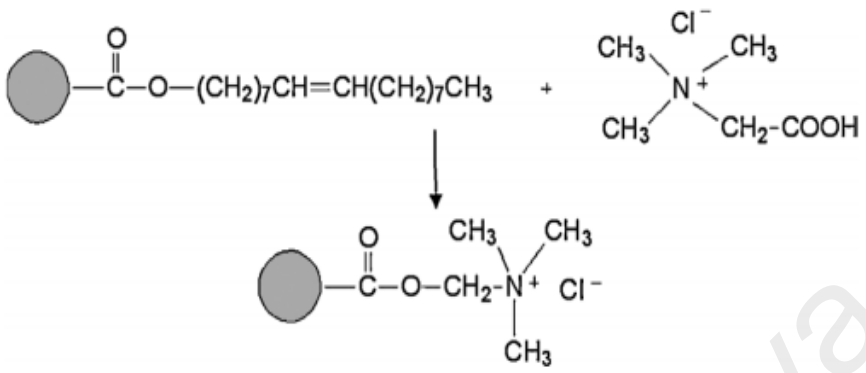

Figure 2.2: Reaction oleic acid with magnetic nanoparticles

(Lee & Harris, 2006)

Refer to the previous study, the coated FNPs showed high magnetization value when compared to the bare NPs due to ease of phase transformation at increased temperature. Other than that, increasing crystallinity size will increase saturation magnetization as well (Rehana, Haleel, & Rahiman, 2015). Petcharoen and Sirivat (2012) also investigated on coated and bare iron oxide NPs. The findings from their research is the oleic acid-coated iron oxide NPs has larger yield than the bare NPs. However, the particle size of the coated FNPs can be reduce with the increment of reaction temperature. The coated FNPs exhibited superparamagnetic at room temperature and showed great suspension stability over 1 week (Petcharoen & Sirivat, 2012).

2.6 Common deposition methods used in iron oxide NPs

Deposition method specially for iron oxide NPs on Si substrate are categorized into several types which are physical vapour deposition (PVD) and chemical vapour deposition (CVD), spin coating and self-assembly. Deposition methods play a vital role in designing of gate dielectric in order to obtain the outstanding physical and electrical characteristics of MOSFET (Chin, Cheong, & Hassan, 2010).

2.6.1 Physical vapour deposition (PVD)

The sub-categories of PVD that mainly used by researchers are sputtering (radio frequency), electron beam evaporation and pulse laser deposition (PLD) (Kawaharamura, 2014). For PLD, it used the technique of laser ablation on the target source. The intense laser beam will vaporize and eject away some of the particles on the surface of target material that eventually deposit on the substrate as a thin film (Chin et al., 2010; Wong & Cheong, 2010). In previous research, PLD is considered as convenient and clean technique to obtain the thin film with high range of compositions, properties and structures (Constantinescu et al., 2012). For electron beam evaporation, the electron beam (E-beam) is employed to heat up of target material in a high-pressure vacuum chamber to produce vaporized material. The vaporized material is then sublimated on the substrate surface to produce a thin film layer through the condensation process (Chin et al., 2010; Wong & Cheong, 2010; D. Zhang, 2011). This deposition method also provides outstanding electrical characteristics due to its ability to have good surface and ultrathin films (D. Zhang, 2011).

Sputtering is one of the PVD process that involved in ejection of source material from the target source. The source material will then deposit onto the substrate placed in vacuum chamber with pressure between 5×10^{-4} to 5×10^{-7} Torr (Chin et al., 2010; Wong & Cheong, 2010). There are two common modes in sputtering namely radio magnetron frequency (RF) sputtering and direct current sputtering. RF sputtering is specifically utilized for target material that has good electrical insulator while DC sputtering for target material with good electrical conductor (Wong & Cheong, 2010). The basic process of sputtering begins when high voltage is exerted on negative-charge (target material) and positive-charge (substrate) to cause a plasma generated from the ionized argon (Ar) gas. The high speed of ionized Ar is then bombarded to the target and result in the ejection of atomic size particles from the target material. The ejected particles are eventually deposited onto the substrate surface as a thin film layer (Chin et al., 2010; Kelly & Arnell, 2000).

In RF magnetron sputtering system, strong magnetic field is used to enhance the electron ionization concentration and extend the travel distance of the electrons, thus improving the ionization and sputtering efficiency (Chin et al., 2010; Maurya, Sardarinejad, & Alameh, 2014). This sputtering method is also suitable for deposition using the non-electrical conductor target materials (Maurya et al., 2014). Based on Wu et al. (2014), RF magnetron sputtering provides a low temperature change of substrate, high deposition rate, well-adhered between thin film and substrate and excellent morphology structure. Besides, some studies also showed that RF magnetron sputtering together with post-deposition annealing or oxidation can improve physical and electrical properties of the thin films while reducing their EOT.

2.6.2 Chemical vapour deposition (CVD)

In CVD, it is divided into two types which are metal organic chemical vapour deposition (MOCVD) and atomic layer deposition (ALD) (Kawaharamura, 2014). MOCVD is one of the CVD methods that involves the decomposition of a metalorganic precursor with a hydride group. The organic gas (H_2 or N_2) will be used to transport the decomposed precursor to the substrate surface and initiate the reaction process (Chin et al., 2010). The advantages of MOCVD are the oxide film able to grow at low temperatures and has a good quality of surface due to its uniform and conform surface coverage (B. P. Zhang, Binh, Segawa, Wakatsuki, & Usami, 2003).

ALD is a chemical gas phase method that involved two complementary precursors. These complementary precursors will then undergo sequential surface reactions process and a conformal thin film is grown on the substrate. The growth of thin film occurs in a cyclic manner which begins with exposing the substrate surface to react with the pulsed first precursors, forming a monolayer on the surface by chemisorption. Then, any excess of the first precursor is purged by inert gas before introducing the second precursor to the substrate. In this stage, the second precursor is pulsed, followed by surface reactions to form another film layer. Lastly, all excess of the second precursor is purged out with the help of inert gas. The cycle will alternately repeated until the desired thickness is achieved (Chin et al., 2010; Päiväsaari, Putkonen, Sajavaara, & Niinistö, 2004; Pessa, Huttunen, & Herman, 1983; Ritala & Leskelä, 2002). In addition, ALD is considered as a promising deposition method due to its capability to achieve good conformality and uniformity of the deposition layer using sequential, self-limiting and self-controlling surface reactions (George, 2010; W.-H. Kim, Maeng, Moon, Myoung, & Kim, 2010).

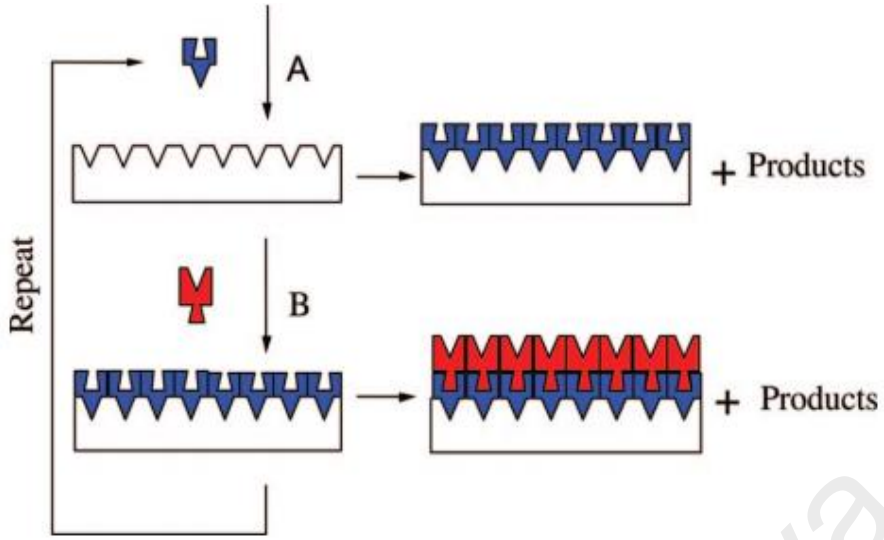

Figure 2.3: Schematic mechanism of ALD cycle

(George, 2010)

2.6.3 Spin coating deposition

This is one of the methods in producing a thin film that involves a process of depositing a small solution when the spin-coater motor is operating at high rotation speed as shown in Figure 2.4. This method also known as on-the-fly-dispensing spin coating approach. The solution will quickly spread over the substrate by finite motor acceleration and a thin film will be formed on the substrate (F. Zhang et al., 2013).

Spin coating enables the successful deposition of thin film on Si substrate due to its simplicity, dry quickly due to high rotation speed, low cos and high consistency at nano length scale (F. Zhang et al., 2013). However, this method is time-consuming as it involved batch process. Besides, the quick-dry literally can lead to the reduction of performance of the MOSFET devices in some of nanotechnology applications.

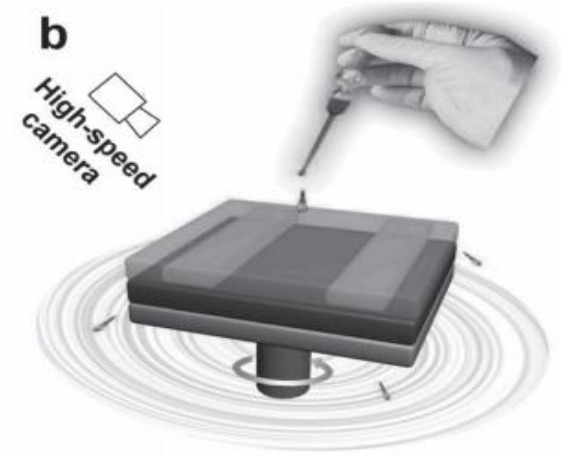

Figure 2.4: Spin coating process

(F. Zhang et al., 2013)

2.6.4 Self-assembly deposition

Self-assembly is a method that involved strong-link chemical with Si substrate which can be done without native oxide, SiO_2 or with SiO_2. For formation of self-assembly monolayers (SAM) with presence of SiO_2, there are three classes of molecules involved and widely used, namely organometallics, silanes and alcohols (Miozzo, Yassar, & Horowitz, 2010). SAM are used in enhancing the performances of the interfaces between dielectric and semiconductor (Baharuddin et al., 2017). The previous study also discussed that controlled oxidation and oxide layer with addition of silanol groups (Si-OH) are important in order to get the ideal surface for SAM growth. Hence, to achieve this result, the Radio Corporation America (RCA) standard method and an ultra-thin layer growth on thermal SiO_2 are recommended to be employed (Baharuddin et al., 2017; Miozzo et al., 2010).

In organic semiconductor aspects, SiO_2 layer is the most popular gate dielectric materials that commonly obtained from the heat treatment of Si substrate. Other than that, the SiO_2 can minimize the leakage currents density and acts as a dynamic dielectric to semiconductor components. However, although the growth of SiO_2 has been optimized to form a defect-free interface when deposited on Si, its top surface particularly for organic field-effect transistor (OFET) is much less defined. Referring to its previous processing, the SiO_2 surface experienced Si-OH defects, leading to trapping and hysteresis of interface. Hence, the synthesizing of SiO_2 often leads to a high degree of variability and low mobility (Miozzo et al., 2010).

2.7 Space-charge-limit conduction

2.7.1 Ohm's Law

In Ohm's Law charge conduction mechanism, the electron is thermally excited and trapped in the bulk oxide at a very low voltage applied. The ohmic contact between oxide and semiconductor formed due to the accumulation of electrons on the gate electrode (Cheong, Moon, Kim, Bahng, & Kim, 2008). Hence, the density of the excited electrons become higher than injected electron from semiconductor which then contributes to the flow of current. However, at this state, not all trap centers are filled with electron due to their weak injection. The linear relationship between the current density and the electric field also can be observed (Wong & Cheong, 2011). Figure 2.5 shows a schematic diagram of the Ohm's Law conduction of electron.

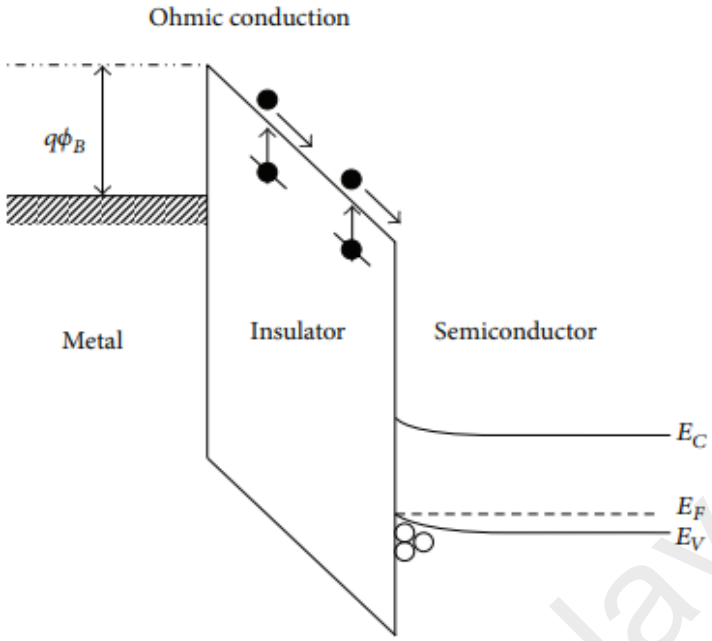

Figure 2.5: Schematic diagram of Ohm's Law conduction of electron (Chiu, Chou, & Lee, 2005)

2.7.2 Poole-Frenkel emission

Poole-Frenkel (PF) emission involves thermal excitation of electrons mechanism which emit out from the traps into the conduction band of oxide. This emission is also known as bulk-limited conduction process (Cheong et al., 2008; Fiorenza, Greco, Giannazzo, Lo Nigro, & Roccaforte, 2012). In this state of emission, the reduction in potential energy will occur and increase the excitation electron out of the trap into the conduction band. The schematic diagram of energy band of PF emission is shown in Figure 2.6.

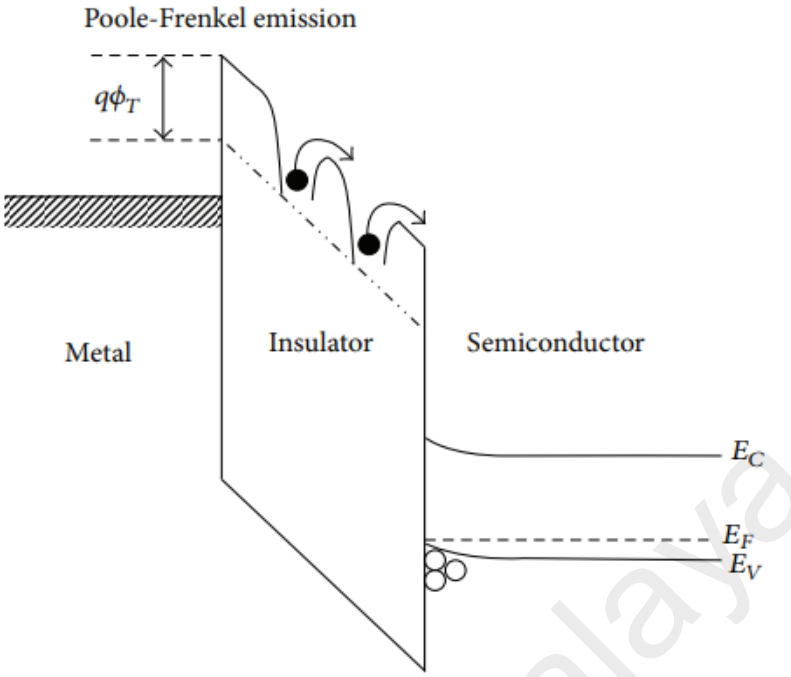

Figure 2.6: Schematic diagram of PF emission

(Chiu et al., 2005)

CHAPTER 3: MATERIALS AND METHODOLOGY

3.1 Introduction

In Chapter 3, it describes the electrical analysis based on charge conduction mechanisms of the Fe_3O_4-γ-Fe_2O_3/SiO_2/n-type Si system. Figure 3.1 represents an overview of this project research. This chapter is divided into two parts:

i. Sample preparation before electrical analysis

ii. Electrical analysis procedures

3.2 Sample preparation before electrical analysis

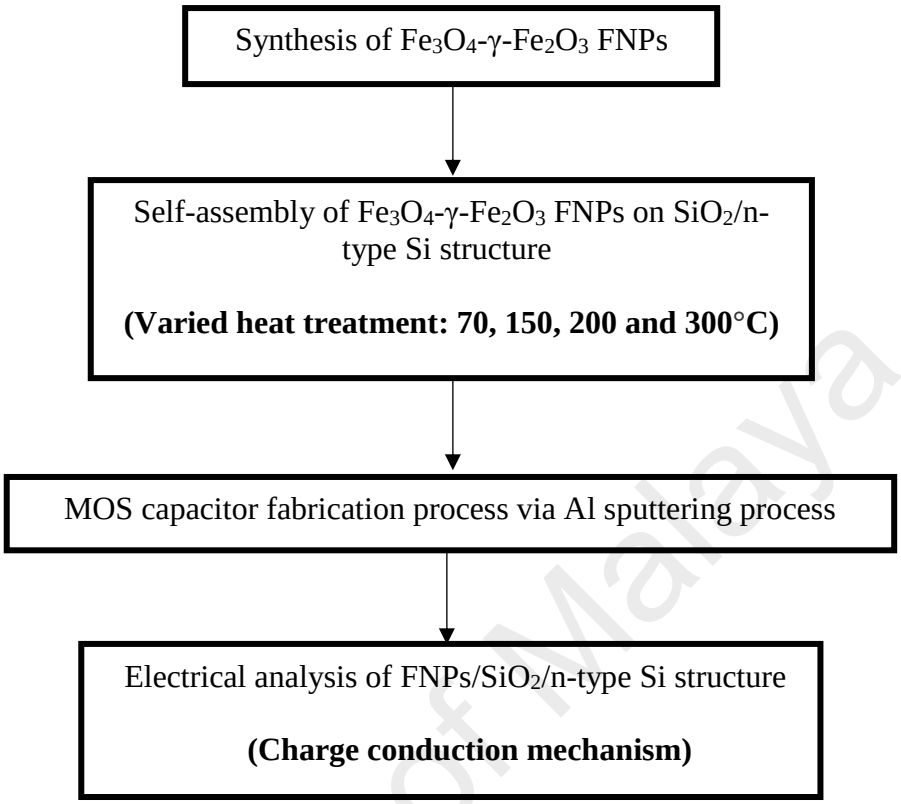

Figure 3.1: Sample preparation of Fe_3O_4-γ-Fe_2O_3 FNPs on SiO_2/n-type Si structure

3.3 Electrical analysis procedures

3.3.1 Charge conduction mechanism characterization

Before J-E graph is plotted, the current-voltage (I-V) using BPW-800 8" probe station along with a Keithley 4200 semiconductor characterization system (SCS). The frequency and sweep range were set to 50 Hz and 0-20 V respectively (Baharuddin et al., 2017). From the J-E plot, the leakage current density at various fields can be obtained. The E value was determined from Equation 3.1:

$$E = \frac{V_g - V_{FB}}{t_{ox}} \tag{3.1}$$

Where V_g is the gate voltage, V_{fb} is the flat band voltage and t_{ox} is the oxide thickness (Goh et al., 2016; Wong & Cheong, 2012).

The charge conduction mechanism was been analysed from the J-E plot data. By using the SigmaPlot, the leakage current density is obtained based on Equation 3.2 and 3.3 as stated below:

$$J_{Ohm} = qn_o \mu V_g / t_{ox} \tag{3.2}$$

$$J_{PF} = (qN_c \mu) E e^{\frac{\left\{-q\left[\emptyset_t - (\frac{qE}{\pi k_r \varepsilon_o})^{1/2}\right]\right\}}{kT}} \tag{3.3}$$

Where q is the electronic charge, n_o is the concentration of charge carriers in thermal equilibrium and μ is the electronic mobility in the oxide, κ is the dielectric constant of the oxide, N_c is the density of states in the conduction band, $\emptyset_t$ is the trap energy level in the oxide, k_r is the dynamic dielectric constant, ε_o is permittivity of free space (8.85 × 10-12 F/m) and T is oxidation temperature (Wong & Cheong, 2011).

From the J_{Ohm} and J_{PF}, the Ohm's Law and PF emission fitted plot are obtained at different oxidation temperature. From the J-V_g plot fitted by Ohm's Law, the slope of the regression line was calculated and comparable with 1. For PF emission plot (ln J/E versus $E^{1/2}$), the slope of regression line at different oxidation temperature was obtained and it represents the dynamic dielectric constant, k_r. Both charge conduction mechanism is been analysed at the leakage current density (J) of the low applied voltage before the electrical breakdown reached.

CHAPTER 4: RESULTS AND DISCUSSION

4.1 Introduction

This chapter discusses and presents the experimental results of the electrical characteristics of the functionalized Fe_3O_4-γ-Fe_2O_3 NPs on SiO_2/n-type Si substrate obtained from the current-voltage (I-V) measurements. In electrical characterization, several charge conduction mechanisms that cause leakage current been analyzed such as Ohm's Law, Child's Law and Poole-Frenkel emission.

4.2 Electrical analysis

4.2.1 J-E characterization

From the I-V measurement obtained from the computer-controlled SPA system, the leakage current density-electric field (J-E) plot is formed of the tested functionalized Fe_3O_4-γ-Fe_2O_3 NPs on SiO_2/n-type Si substrate. The plotted J-E graph is purposely to study the effects of oxidation temperature on the electrical properties of the samples. All of the samples demonstrate an electrical breakdown field (E_B) which indicated the increments of leakage current densities. At E_B, the instantaneous increment in leakage current density is observed to be relatively small compared to another electric field. Hence, the leakage current condition that cause E_B is been investigated from the charge conduction mechanisms through the oxides. Based on J-E plot (Figure 4.1), the sample heat-treated at 150^{o}C shows the highest E_B followed by the samples heated at 70^{o}C, 200^{o}C and 300^{o}C with E_B values of 2.57×10^{-3}, 1.85×10^{-3}, 1.45×10^{-3}, and $1.10 \times$

10^{-3} MV/cm respectively. This variation can be related to their surface roughness which already been investigated previously (Baharuddin et al., 2017). At the highest RMS roughness value at 18.12 ± 7.13 nm., the heat-treated sample of 150°C showed the most encouraging E_B while for sample heated at 300°C, it has the lower RMS value 13.58 ± 4.03 nm and possessed the lowest E_B. Besides, it can also be concluded that when the electric field increase, the longer it takes for the oxide layer to breakdown.

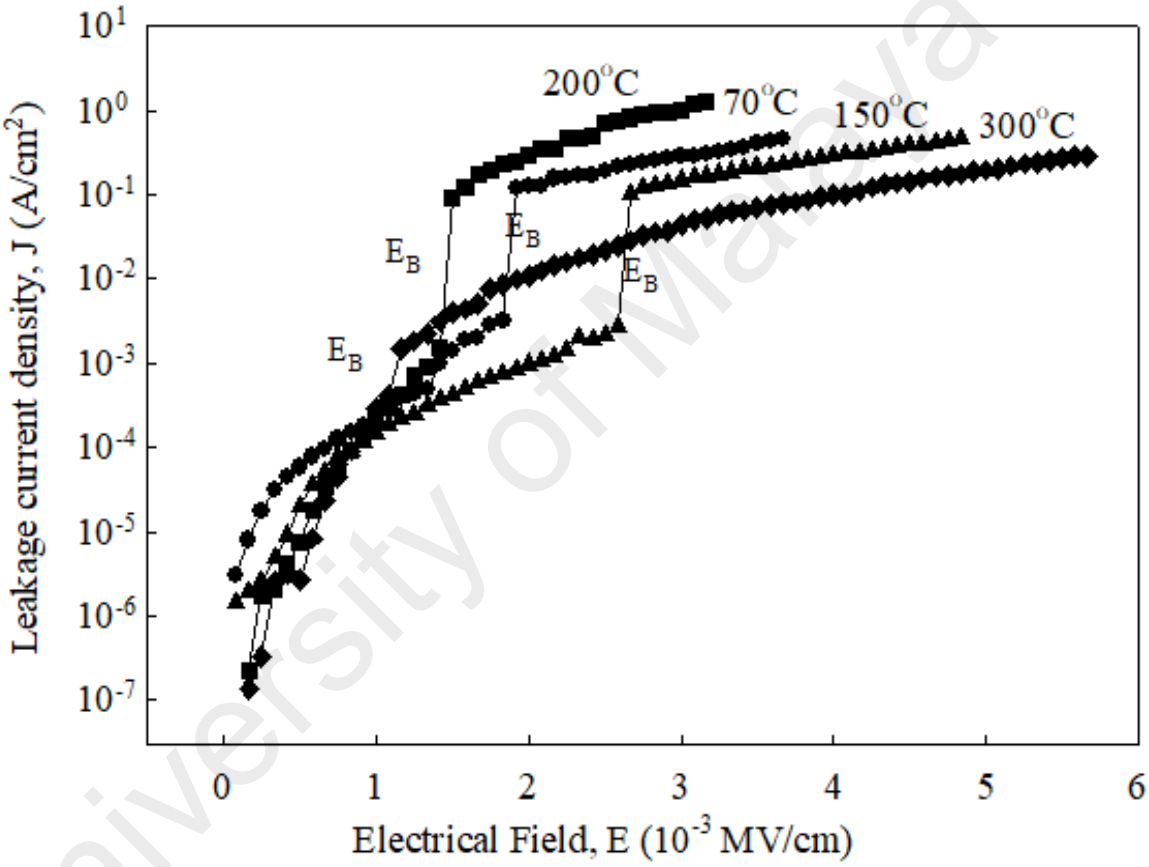

Figure 4.1: J-E characteristics at different temperature

4.3 Charge conduction mechanism

In this study, several possible charge conduction mechanisms that create the leakage current density has been investigated on the functionalized Fe_3O_4-γ-Fe_2O_3 NPs on SiO_2/n-type Si substrate. As positive gate voltage is applied on the gate electrode, electrons as the majority carriers n-type Si are being accumulated. Thus, it forms Ohmic contact between the oxide and semiconductor. The injection of electrons into oxide occurs at the very low gate voltage when the density of the accumulated electrons in oxide is higher than the density of the accumulated electrons in the forward-biased semiconductor. Then, at high voltage, the electrons will be tunneled through the oxide.

Based on Lampert's theory, it is stated that low density of free carriers is formed due to the states of impurity and defect in the insulators and produced the unbalance charge by the electric fields as the injection of electrons occurred. The continuous injection of electrons will then cause the formation of a space charge region which later hinders further injection of electrons into oxide.

4.3.1 Space-charge-limited conduction

In Lampert's theory of space-charge-limited-conduction (SCLC) at low voltage, there are three limiting mechanisms (Ohm's Law, trap-filled limit (TFL) conduction and Child's Law) involved in current density-voltage (J-V) characteristics. In this study, only Ohm's Law have been investigated to identify the leakage current path of the samples of the functionalized Fe_3O_4-γ-Fe_2O_3 NPs on SiO_2/n-type Si substrate. The SCLC will be increased when the interface trap density of oxide and semiconductor is increase.

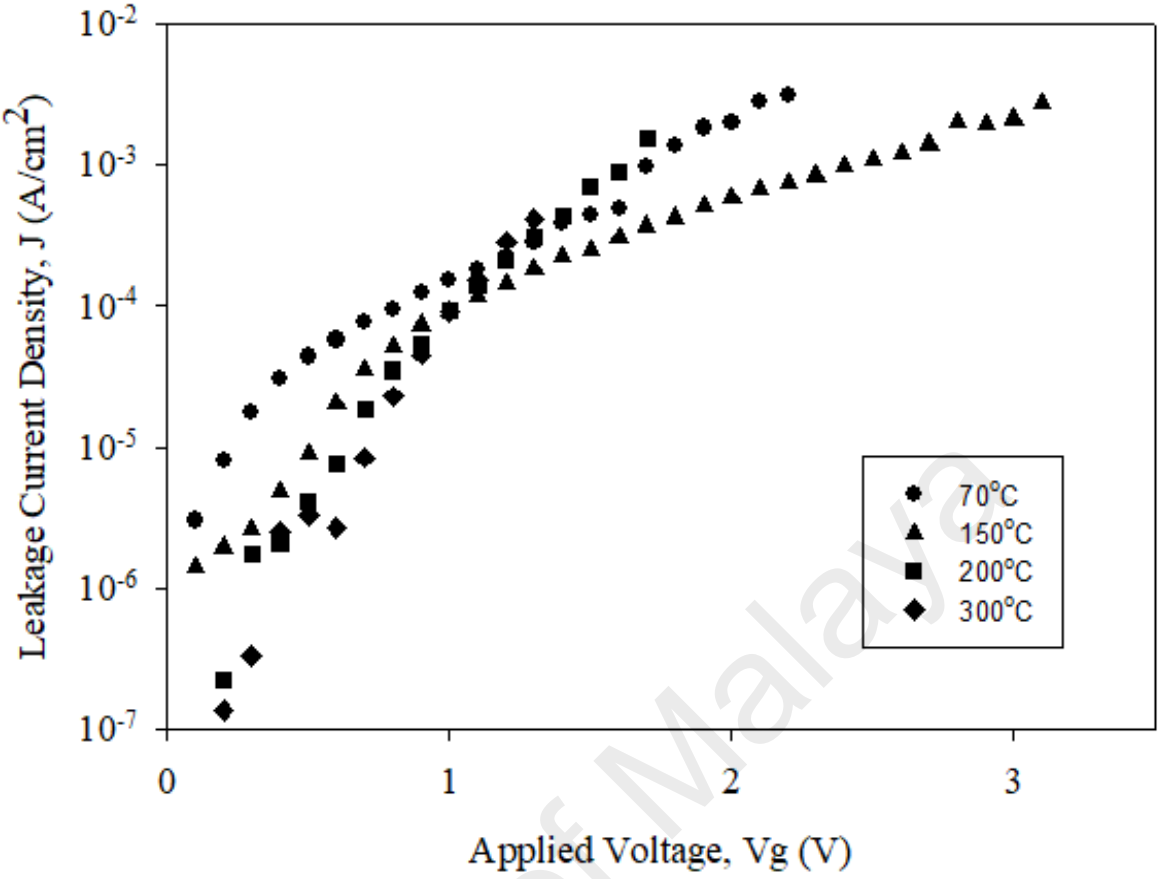

Figure 4.2: J-V_g graph at different temperature

4.3.1.1 Ohm's Law

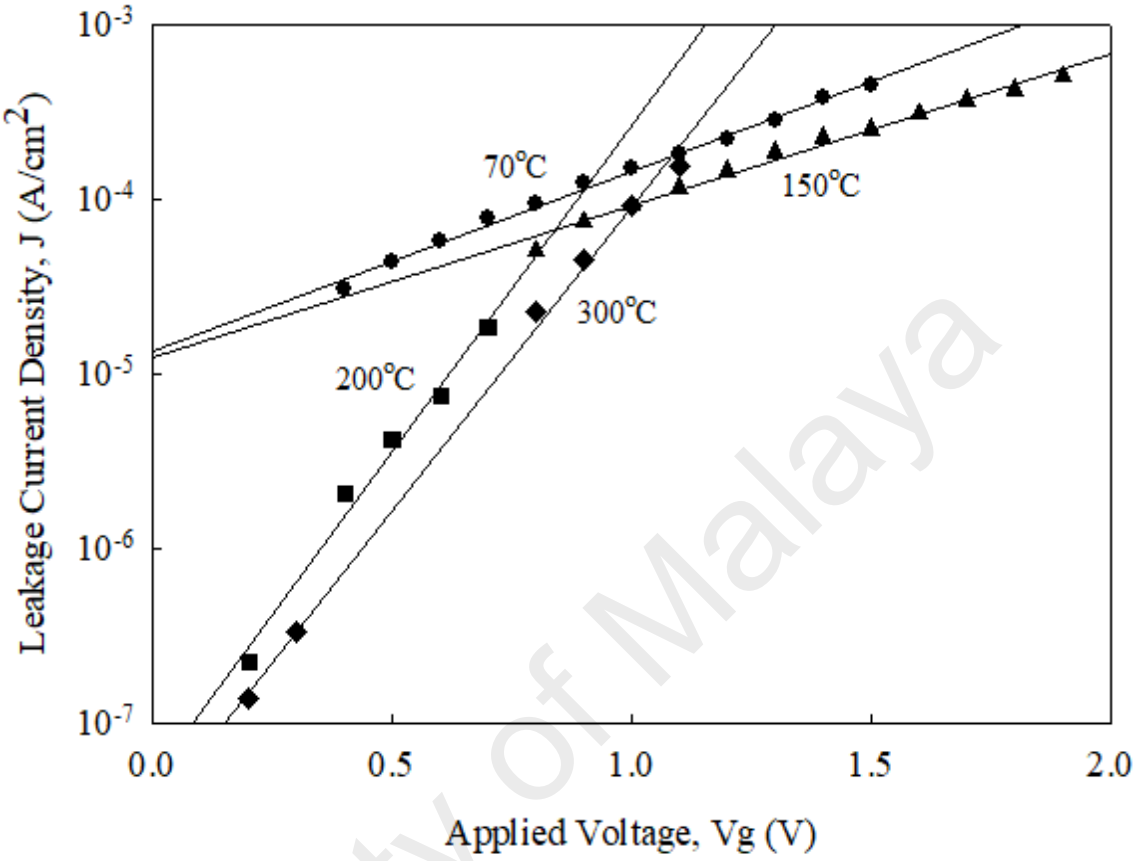

Figure 4.3: J-V_g plot fitted by Ohm's Law at different temperatures

Figure 4.3 shows J-V plot fitted with Ohm's Law measured at different temperature. The data is initially identified from the low voltage applied to the gate semiconductor as shown in Figure 4.2. The slope of fitted been obtained and comparable with 1. The extracted slope values are presented in Figure 4.4 as a function of oxidation temperature. Sample heated at 70°C and 150°C have a slope close to 1. Hence, it can be concluded that they obeyed the Ohm's Law. However, the samples heated with 200°C and 300°C showed the slope higher than 1 which is 3.47 and 3.73 respectively. From the data obtained, they are considered not obey the Ohm's Law. It is due to very high electrical resistance experienced by them and lower electrical breakdown, E_B. Besides,

the obtained data also can be related to the surface characterization by the previous study. Baharuddin et al. (2017) stated that the surface roughness of iron oxide NPs plays an important role in electrical characterization. The findings stated that sample with heat treatment of 200°C and 300°C resulted in declination of surface roughness which lowering the attachment of aggregated NPs and decrease the electrical breakdown field for both samples. Meanwhile, for sample heated at 150°C, it displayed the highest electrical breakdown, E_B and has the highest surface roughness which related to the highest aggregation NPs.

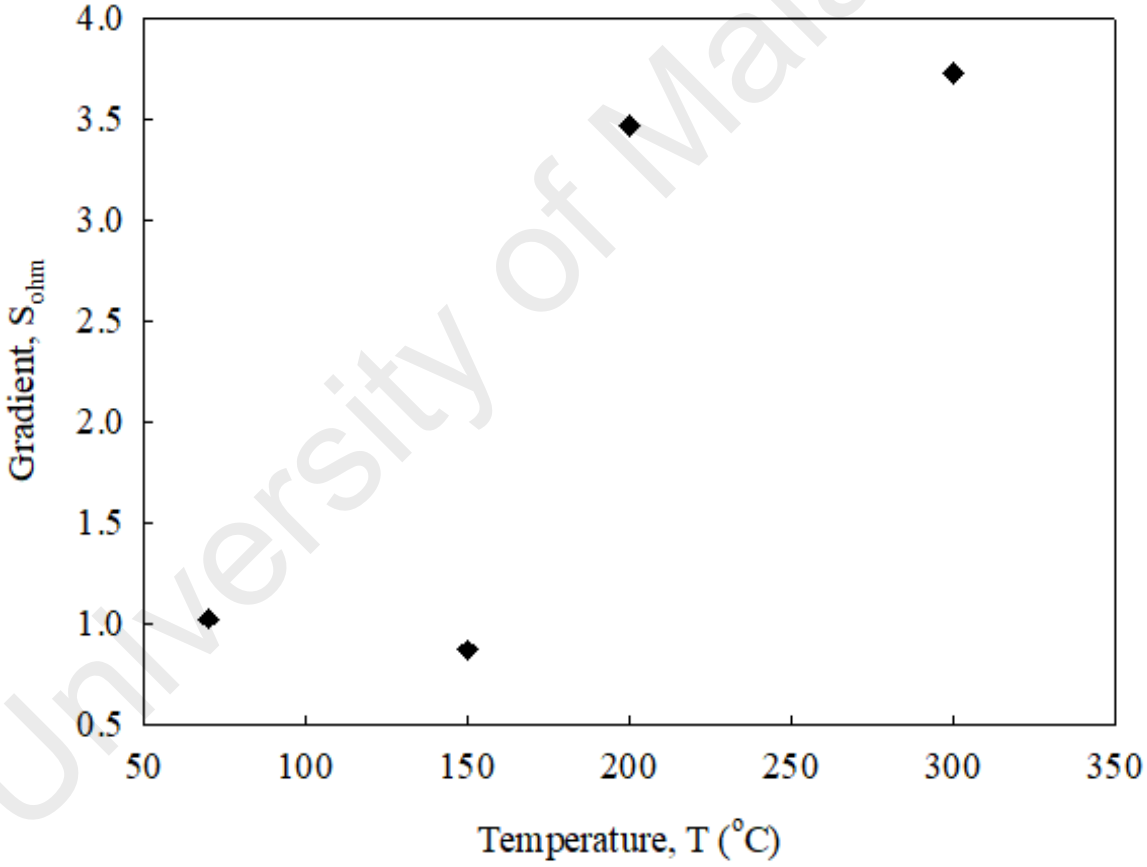

Figure 4.4: Gradient of J-V_g plot fitted with Ohm's Law

4.3.2 Poole-Frenkel emission

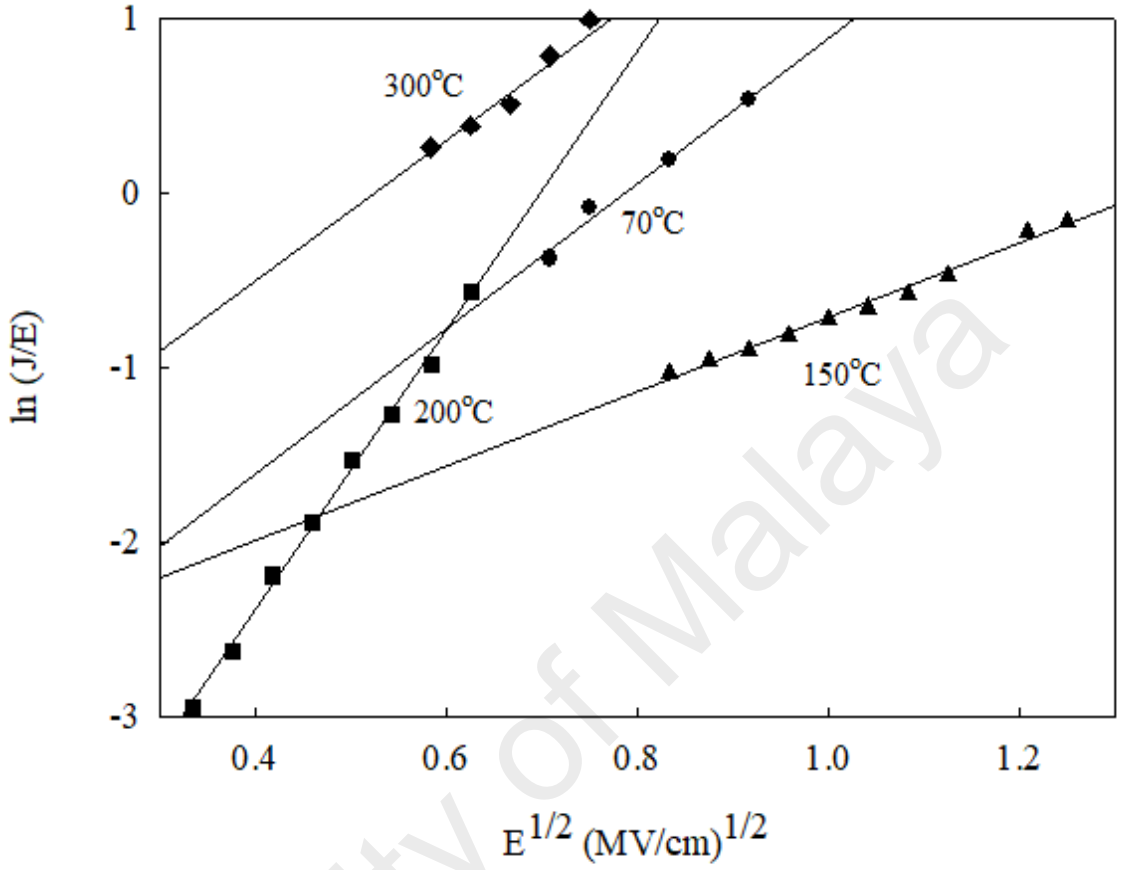

Figure 4.5: PF emission plot at different temperature

Figure 4.7 showed the leakage current density from PF emission plot. The data fall on the straight lines when plotted under ln (J/E) against $E^{1/2}$ with r^2 between 0.97-0.99. The leakage current density at high voltage is observed in analyzing the PF emission of conduction mechanism at various temperature. The slope of PF lines is calculated to obtained the value of dynamic dielectric constant, k_r. The highest of k_r (7.99) is presented by a heat-treated sample of 200°C followed by 70°C (4.34), 150°C (3.85) and 300°C (2.97) respectively. This variation showed the relationship between dynamic dielectric constant and electrical breakdown, E_B of the heat-treated samples. Based on Figure 4.8, the heat-treated sample of 200°C revealed the encouraging k_r which makes it suitable to

be used as the gate dielectric as its dielectric constant is higher than SiO_2. However, the E_B is considered as lower compared to 70ºC and 150ºC and produced more leakage current at the oxide layer. However, the situation differs in a heated sample of 150ºC where it produces the highest E_B and acceptable k_r (same as k of SiO_2). Thus, a heat-treated sample of 150ºC is considered to have good electrical properties in terms of electrical breakdown and dynamic dielectric constant.

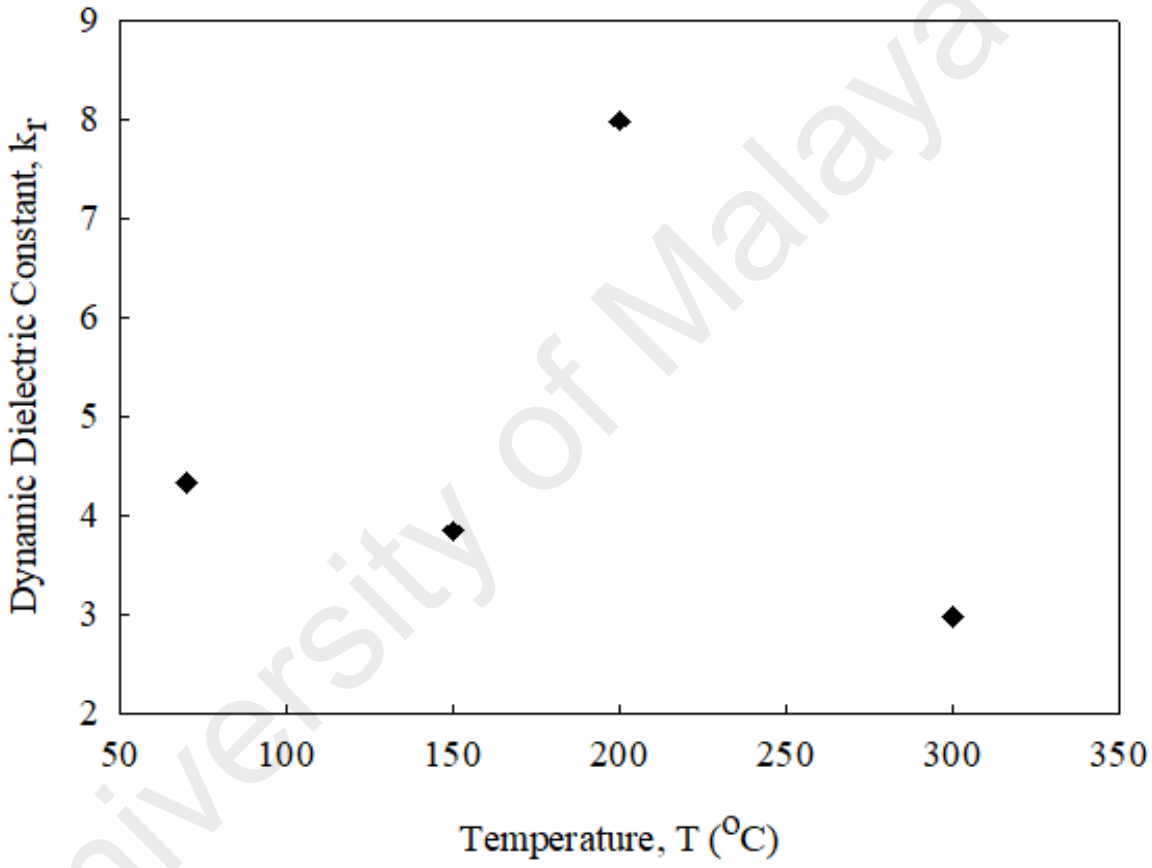

Figure 4.6: k_r from PF emission plot of different temperatures

CHAPTER 5: CONCLUSIONS

5.1 Conclusions

In electrical characterization of self-assembled 4-pentynoic acid functionalized Fe_3O_4-γ-Fe_2O_3 NPs on SiO_2/n-Si substrate, the charge conduction mechanisms were quantitatively investigated and analyzed through the oxides. The self-assembly of iron oxide NPs and charge conduction mechanisms through the oxide were affected by different heat treatment temperatures (70-300^oC). The J-E measurements extracted from I-V curves been fitted with different mechanisms of charge conduction. In this study, the Ohm's Law and PF emission are intensively investigated to identify the leakage current density of the tested materials. At the lower electric field, the leakage current due to Ohm's law is the major sources contributing to oxide breakdown at the electrical breakdown field, E_B level. On the other hand, the PF emission is identified and analyzed at the higher electric field. The highest E_B was accredited to the heat-treated sample of 150^oC with values of 2.58×10^{-3} MV/cm approximately at 10^{-3} A/cm^2 and it obeys the Ohm's law as the slope is near to 1. For dynamic dielectric constant (k_r), the sample heated at 200^oC showed promising value compared to other temperatures and acquired *k*-value (7.99) higher than commercial native oxide, SiO_2 (3.8-3.9). However, its E_B is considered low which limits its performance electrically. Besides, the heat-treated sample of 150^oC demonstrated the best outcomes as the leakage current is low (10^{-3} A/cm^2), high E_B (2.58×10^{-3} MV/cm), has k_r close to *k* of SiO_2 (3.85) and attained the highest barrier height (0.38 eV) (Baharuddin et al., 2017).

5.2 Recommendations for future work

Several suggestions for future study related to the functionalized Fe_3O_4-γ-Fe_2O_3 NPs on SiO_2/n-Si substrate is:

i. Charge conduction mechanism of trap-filled limit and trap-assisted tunneling mechanism need to be carried out in order to compare the trend of interface trap and electric field breakdown.

ii. The thickness of SiO_2 using transmission electron microscopy need to be analysed to attain more precise oxide breakdown field and barrier height.

iii. Mechanical analysis on hardness, toughness and tensile strength of the functionalized Fe_3O_4-γ-Fe_2O_3 NPs on SiO_2/n-Si substrate need to be studied since the references are still limited.

REFERENCES

Akbarzadeh, A., Samiei, M., & Davaran, S. (2012). Magnetic nanoparticles: preparation, physical properties, and applications in biomedicine. *Nanoscale research letters, 7*(1), 144-144. doi:10.1186/1556-276X-7-144

Ar, N., S, T., M, S., Sss, A., & Sm, M. H. (2017). Iron Oxide Biomagnetic Nanoparticles (IO-BMNPs); Synthesis, Characterization and Biomedical Application–A Review. *Journal of Nanomedicine & Nanotechnology, 08*(01). doi:10.4172/2157-7439.1000423

Baharuddin, A. A., Ang, B. C., & Wong, Y. H. (2017). Self-assembly and electrical characteristics of 4-pentynoic acid functionalized Fe3O4-γ-Fe2O3 nanoparticles on SiO2/n-Si. *Applied Surface Science, 423*, 236-244. doi:10.1016/j.apsusc.2017.06.155

Bohr, M. (2009, 8-12 Feb. 2009). *The new era of scaling in an SoC world.* Paper presented at the 2009 IEEE International Solid-State Circuits Conference - Digest of Technical Papers.

Bohr, M. T., & Young, I. A. (2017). CMOS Scaling Trends and Beyond. *IEEE Micro, 37*(6), 20-29. doi:10.1109/MM.2017.4241347

Brassard, D., Sarkar, D. K., El Khakani, M. A., & Ouellet, L. (2004). High-k titanium silicate thin films grown by reactive magnetron sputtering for complementary metal–oxide–semiconductor applications. *Journal of Vacuum Science & Technology A: Vacuum, Surfaces, and Films, 22*(3). doi:10.1116/1.1722530

Chaudhry, A., & Roy, J. N. (2010). [Mosfet Models, Quantum Mechanical Effects and Modeling Approaches: A Review]. *10*. doi:10.5573/JSTS.2010.10.1.020

Cheong, K. Y., Moon, J. H., Kim, H. J., Bahng, W., & Kim, N.-K. (2008). Current conduction mechanisms in atomic-layer-deposited HfO2/nitrided SiO2 stacked gate on 4H silicon carbide. *Journal of Applied Physics, 103*(8). doi:10.1063/1.2908870

Chin, W. C., Cheong, K. Y., & Hassan, Z. (2010). Sm2O3 gate dielectric on Si substrate. *Materials Science in Semiconductor Processing, 13*(5-6), 303-314. doi:10.1016/j.mssp.2011.02.001

Chiu, F.-C., Chou, H.-W., & Lee, J. Y.-m. (2005). Electrical conduction mechanisms of metal/La2O3/Si structure. *Journal of Applied Physics, 97*(10). doi:10.1063/1.1896435

Chiu, F.-C., & Lai, C.-M. (2010). Optical and electrical characterizations of cerium oxide thin films. *Journal of Physics D: Applied Physics, 43*(7). doi:10.1088/0022-3727/43/7/075104

Constantinescu, C., Ion, V., Galca, A. C., & Dinescu, M. (2012). Morphological, optical and electrical properties of samarium oxide thin films. *Thin Solid Films, 520*(20), 6393-6397. doi:10.1016/j.tsf.2012.06.049

Cui, Y., & Lieber, C. M. (2001). Functional nanoscale electronic devices assembled using silicon nanowire building blocks. *Science, 291*(5505), 851-853. doi:10.1126/science.291.5505.851

Darroudi, M., Hakimi, M., Goodarzi, E., & Kazemi Oskuee, R. (2014). Superparamagnetic iron oxide nanoparticles (SPIONs): Green preparation, characterization and their cytotoxicity effects. *Ceramics International, 40*(9), 14641-14645. doi:10.1016/j.ceramint.2014.06.051

Esro, M., Vourlias, G., Somerton, C., Milne, W. I., & Adamopoulos, G. (2015). High-Mobility ZnO Thin Film Transistors Based on Solution-processed Hafnium Oxide Gate Dielectrics. *Advanced Functional Materials, 25*(1), 134-141. doi:10.1002/adfm.201402684

Filippousi, M., Angelakeris, M., Katsikini, M., Paloura, E., Efthimiopoulos, I., Wang, Y., . . . Van Tendeloo, G. (2014). Surfactant Effects on the Structural and Magnetic Properties of Iron Oxide Nanoparticles. *The Journal of Physical Chemistry C, 118*(29), 16209-16217. doi:10.1021/jp5037266

Fiorenza, P., Greco, G., Giannazzo, F., Lo Nigro, R., & Roccaforte, F. (2012). Poole-Frenkel emission in epitaxial nickel oxide on AlGaN/GaN heterostructures. *Applied Physics Letters, 101*(17). doi:10.1063/1.4761961

George, S. M. (2010). Atomic Layer Deposition: An Overview. *Chemical Reviews, 110*(1), 111-131. doi:10.1021/cr900056b

Goh, K. H., Haseeb, A. S. M. A., & Wong, Y. H. (2016). Physical and electrical properties of thermal oxidized Sm2O3 gate oxide thin film on Si substrate: Influence of oxidation durations. *Thin Solid Films, 606,* 80-86. doi:10.1016/j.tsf.2016.03.051

Guardia, P., Labarta, A., & Batlle, X. (2011). Tuning the Size, the Shape, and the Magnetic Properties of Iron Oxide Nanoparticles. *The Journal of Physical Chemistry C, 115*(2), 390-396. doi:10.1021/jp1084982

Gubin, S. P., Koksharov, Y. A., Khomutov, G. B., & Yurkov, G. Y. (2005). Magnetic nanoparticles: preparation, structure and properties. *Russian Chemical Reviews, 74*(6), 489-520. doi:10.1070/RC2005v074n06ABEH000897

Gupta, A. K., & Gupta, M. (2005). Synthesis and surface engineering of iron oxide nanoparticles for biomedical applications. *Biomaterials, 26*(18), 3995-4021. doi:10.1016/j.biomaterials.2004.10.012

Heng, G. K. (2017). *Samarium oxide and samarium oxynitride thin film gate oxides on silicon substrate.* University of Malaya,

Jeliazova, Y., Kayser, M., Mildner, B., Hassel, A. W., & Diesing, D. (2006). Temperature stability of thin anodic oxide films in metal/insulator/metal structures: A comparison between tantalum and aluminium oxide. *Thin Solid Films, 500*(1-2), 330-335. doi:10.1016/j.tsf.2005.10.088

Jing, J., Zhang, Y., Liang, J., Zhang, Q., Bryant, E., Avendano, C., . . . Yu, W. W. (2012). One-step reverse precipitation synthesis of water-dispersible superparamagnetic

magnetite nanoparticles. *Journal of Nanoparticle Research, 14*(4). doi:10.1007/s11051-012-0827-3

Kamata, Y., Kamimuta, Y., Ino, T., & Nishiyama, A. (2005). Direct Comparison of ZrO2and HfO2on Ge Substrate in Terms of the Realization of Ultrathin High-κ Gate Stacks. *Japanese Journal of Applied Physics, 44*(4B), 2323-2329. doi:10.1143/jjap.44.2323

Kawaharamura, T. (2014). Physics on development of open-air atmospheric pressure thin film fabrication technique using mist droplets: Control of precursor flow. *Japanese Journal of Applied Physics, 53*(5S1). doi:10.7567/jjap.53.05ff08

Kelly, P. J., & Arnell, R. D. (2000). Magnetron sputtering: a review of recent developments and applications. *Vacuum, 56*(3), 159-172. doi:https://doi.org/10.1016/S0042-207X(99)00189-X

Khalil, M., Yu, J., Liu, N., & Lee, R. L. (2014). Non-aqueous modification of synthesized hematite nanoparticles with oleic acid. *Colloids and Surfaces A: Physicochemical and Engineering Aspects, 453*, 7-12. doi:10.1016/j.colsurfa.2014.03.064

Kim, S., Konar, A., Hwang, W. S., Lee, J. H., Lee, J., Yang, J., . . . Kim, K. (2012). High-mobility and low-power thin-film transistors based on multilayer MoS2 crystals. *Nat Commun, 3*, 1011. doi:10.1038/ncomms2018

Kim, W.-H., Maeng, W. J., Moon, K.-J., Myoung, J.-M., & Kim, H. (2010). Growth characteristics and electrical properties of La2O3 gate oxides grown by thermal

and plasma-enhanced atomic layer deposition. *Thin Solid Films, 519*(1), 362-366. doi:10.1016/j.tsf.2010.07.108

Lee, S. Y., & Harris, M. T. (2006). Surface modification of magnetic nanoparticles capped by oleic acids: characterization and colloidal stability in polar solvents. *J Colloid Interface Sci, 293*(2), 401-408. doi:10.1016/j.jcis.2005.06.062

Li, X.-M., Xu, G., Liu, Y., & He, T. (2011). Magnetic Fe3O4 Nanoparticles: Synthesis and Application in Water Treatment. *Nanoscience & Nanotechnology-Asia, 1*(1), 14-24. doi:10.2174/2210681211101010014

Li, Y., Guo, W., Wu, Z., Jin, L., Ke, Y., Guo, Q., & Hu, S. (2016). Determination of ultra-trace rare earth elements in high-salt groundwater using aerosol dilution inductively coupled plasma-mass spectrometry (ICP-MS) after iron hydroxide co-precipitation. *Microchemical Journal, 126*, 194-199. doi:10.1016/j.microc.2015.12.006

Liao, L., Lin, Y. C., Bao, M., Cheng, R., Bai, J., Liu, Y., . . . Duan, X. (2010). High-speed graphene transistors with a self-aligned nanowire gate. *Nature, 467*(7313), 305-308. doi:10.1038/nature09405

Lu, A. H., Salabas, E. L., & Schuth, F. (2007). Magnetic nanoparticles: synthesis, protection, functionalization, and application. *Angew Chem Int Ed Engl, 46*(8), 1222-1244. doi:10.1002/anie.200602866

Mahdavi, M., Ahmad, M. B., Haron, M. J., Namvar, F., Nadi, B., Rahman, M. Z., & Amin, J. (2013). Synthesis, surface modification and characterisation of biocompatible magnetic iron oxide nanoparticles for biomedical applications. *Molecules, 18*(7), 7533-7548. doi:10.3390/molecules18077533

Mahmoudi, M., Sant, S., Wang, B., Laurent, S., & Sen, T. (2011). Superparamagnetic iron oxide nanoparticles (SPIONs): development, surface modification and applications in chemotherapy. *Adv Drug Deliv Rev, 63*(1-2), 24-46. doi:10.1016/j.addr.2010.05.006

Maurya, D., Sardarinejad, A., & Alameh, K. (2014). Recent Developments in R.F. Magnetron Sputtered Thin Films for pH Sensing Applications—An Overview. *Coatings, 4*(4), 756-771. doi:10.3390/coatings4040756

Miozzo, L., Yassar, A., & Horowitz, G. (2010). Surface engineering for high performance organic electronic devices: the chemical approach. *Journal of Materials Chemistry, 20*(13). doi:10.1039/b922385a

Misra, D., Iwai, H., & Wong, H. (2005). High-k Gate Dielectrics. *Electrochemical Society Interface, 14*(2), 30-34. Retrieved from http://www.scopus.com/inward/record.url?scp=23244462592&partnerID=8YFLogxK

Ng, K. K., & Lynch, W. T. (1987). The impact of intrinsic series resistance on MOSFET scaling. *IEEE Transactions on Electron Devices, 34*(3), 503-511. doi:10.1109/T-ED.1987.22956

Päiväsaari, J., Putkonen, M., Sajavaara, T., & Niinistö, L. (2004). Atomic layer deposition of rare earth oxides: erbium oxide thin films from β-diketonate and ozone precursors. *Journal of Alloys and Compounds, 374*(1), 124-128. doi:https://doi.org/10.1016/j.jallcom.2003.11.149

Pang, Y. L., Lim, S., Ong, H. C., & Chong, W. T. (2016). Research progress on iron oxide-based magnetic materials: Synthesis techniques and photocatalytic applications. *Ceramics International, 42*(1), 9-34. doi:10.1016/j.ceramint.2015.08.144

Pessa, M., Huttunen, P., & Herman, M. A. (1983). Atomic layer epitaxy and characterization of CdTe films grown on CdTe (110) substrates. *Journal of Applied Physics, 54*(10), 6047-6050. doi:10.1063/1.331751

Petcharoen, K., & Sirivat, A. (2012). Synthesis and characterization of magnetite nanoparticles via the chemical co-precipitation method. *Materials Science and Engineering: B, 177*(5), 421-427. doi:10.1016/j.mseb.2012.01.003

Rahdar, A., Taboada, P., Aliahmad, M., Hajinezhad, M. R., & Sadeghfar, F. (2018). Iron oxide nanoparticles: Synthesis, physical characterization, and intraperitoneal biochemical studies in Rattus norvegicus. *Journal of Molecular Structure, 1173*, 240-245. doi:10.1016/j.molstruc.2018.06.098

Rashdan, S., Bououdina, M., & Al-Saie, A. (2013). Effect of the preparation route, PEG and annealing on the phase stability of Fe3O4 nanoparticles and their magnetic

properties. *Journal of Experimental Nanoscience, 8*(2), 210-222. doi:10.1080/17458080.2011.566632

Rehana, D., Haleel, A. K., & Rahiman, A. K. (2015). Hydroxy, carboxylic and amino acid functionalized superparamagnetic iron oxide nanoparticles: Synthesis, characterization and in vitro anti-cancer studies. *Journal of Chemical Sciences, 127*(7), 1155-1166. doi:10.1007/s12039-015-0876-0

Riaz, S., Bashir, M., & Naseem, S. (2014). Iron Oxide Nanoparticles Prepared by Modified Co-Precipitation Method. *IEEE Transactions on Magnetics, 50*(1), 1-4. doi:10.1109/tmag.2013.2277614

Ritala, M., & Leskelä, M. (2002). Chapter 2 - Atomic layer deposition. In H. Singh Nalwa (Ed.), *Handbook of Thin Films* (pp. 103-159). Burlington: Academic Press.

Robertson, J. (2004). High dielectric constant oxides. *The European Physical Journal Applied Physics, 28*(3), 265-291. doi:10.1051/epjap:2004206

Robertson, J., & Wallace, R. M. (2015). High-K materials and metal gates for CMOS applications. *Materials Science and Engineering: R: Reports, 88*, 1-41. doi:10.1016/j.mser.2014.11.001

Salmani-Jelodar, M., Ilatikhameneh, H., Kim, S., Ng, K., Sarangapani, P., & Klimeck, G. (2016). Optimum High-k Oxide for the Best Performance of Ultra-Scaled Double-Gate MOSFETs. *IEEE Transactions on Nanotechnology, 15*(6), 904-910. doi:10.1109/tnano.2016.2583411

Sayed, M. A. E., & Atef, M. (2005). Study of tunneling current through ultra-thin gate oxide MOSFET and its effect on CMOS circuits. *Journal of Engineering Sciences, Assiut University, 33*, 929-941.

Shete, P. B., Patil, R. M., Tiwale, B. M., & Pawar, S. H. (2015). Water dispersible oleic acid-coated Fe3O4 nanoparticles for biomedical applications. *Journal of Magnetism and Magnetic Materials, 377*, 406-410. doi:10.1016/j.jmmm.2014.10.137

Smit, M., van der Tol, J., & Hill, M. (2012). Moore's law in photonics. *Laser & Photonics Reviews, 6*(1), 1-13. doi:10.1002/lpor.201100001

Soares, P. I., Alves, A. M., Pereira, L. C., Coutinho, J. T., Ferreira, I. M., Novo, C. M., & Borges, J. P. (2014). Effects of surfactants on the magnetic properties of iron oxide colloids. *J Colloid Interface Sci, 419*, 46-51. doi:10.1016/j.jcis.2013.12.045

Soares, P. I., Lochte, F., Echeverria, C., Pereira, L. C., Coutinho, J. T., Ferreira, I. M., . . . Borges, J. P. (2015). Thermal and magnetic properties of iron oxide colloids: influence of surfactants. *Nanotechnology, 26*(42), 425704. doi:10.1088/0957-4484/26/42/425704

Vangijzegem, T., Stanicki, D., & Laurent, S. (2019). Magnetic iron oxide nanoparticles for drug delivery: applications and characteristics. *Expert Opin Drug Deliv, 16*(1), 69-78. doi:10.1080/17425247.2019.1554647

Wilk, G., Wallace, R., & Anthony, J. (2001). High-?? Gate Dielectrics: Current Status and Materials Properties Considerations. *Journal of Applied Physics, 89*, 5243-5275. doi:10.1063/1.1361065

Williams, R. S. (2017). What's Next? [The end of Moore's law]. *Computing in Science & Engineering, 19*(2), 7-13. doi:10.1109/MCSE.2017.31

Wong, Y. H., & Cheong, K. Y. (2010). ZrO2 thin films on Si substrate. *Journal of Materials Science: Materials in Electronics, 21*(10), 980-993. doi:10.1007/s10854-010-0144-5

Wong, Y. H., & Cheong, K. Y. (2011). Electrical Characteristics of Oxidized/Nitrided Zr Thin Film on Si. *Journal of The Electrochemical Society, 158*(12). doi:10.1149/2.106112jes

Wong, Y. H., & Cheong, K. Y. (2012). Properties of thermally oxidized and nitrided Zr-oxynitride thin film on 4H–SiC in diluted N2O ambient. *Materials Chemistry and Physics, 136*(2-3), 624-637. doi:10.1016/j.matchemphys.2012.07.035

Wong, Y. H., & Cheong, K. Y. (2013). Comparison of oxidized/nitrided Zr thin films on Si and SiC substrates. *Ceramics International, 39*, S475-S479. doi:10.1016/j.ceramint.2012.10.117

Woo, K., Hong, J., Choi, S., Lee, H.-W., Ahn, J.-P., Kim, C. S., & Lee, S. W. (2004). Easy Synthesis and Magnetic Properties of Iron Oxide Nanoparticles. *Chemistry of Materials, 16*(14), 2814-2818. doi:10.1021/cm049552x

Wu, Y., Zhu, S., Liu, T., Li, F., Zhang, Y., Rao, Y., & Zhang, Y. (2014). Preparation and properties of erbium oxide films deposited by radio frequency magnetron sputtering. *Applied Surface Science, 307*, 615-620. doi:10.1016/j.apsusc.2014.04.086

Yeo, Y.-C., King, T.-J., & Hu, C. (2002). Direct tunneling leakage current and scalability of alternative gate dielectrics. *Applied Physics Letters, 81*(11), 2091-2093. doi:10.1063/1.1506941

Zhang, B. P., Binh, N. T., Segawa, Y., Wakatsuki, K., & Usami, N. (2003). Optical properties of ZnO rods formed by metalorganic chemical vapor deposition. *Applied Physics Letters, 83*(8), 1635-1637. doi:10.1063/1.1605803

Zhang, D. (2011). Thermal barrier coatings prepared by electron beam physical vapor deposition (EB–PVD). In *Thermal Barrier Coatings* (pp. 3-24).

Zhang, F., Di, C. A., Berdunov, N., Hu, Y., Hu, Y., Gao, X., . . . Zhu, D. (2013). Ultrathin film organic transistors: precise control of semiconductor thickness via spin-coating. *Adv Mater, 25*(10), 1401-1407. doi:10.1002/adma.201204075

Zhang, Y., Kohler, N., & Zhang, M. (2002). Surface modification of superparamagnetic magnetite nanoparticles and their intracellular uptake. *Biomaterials, 23*(7), 1553-1561. doi:https://doi.org/10.1016/S0142-9612(01)00267-8

Zhou, Z., Wu, C., Liu, H., Zhu, X., Zhao, Z., Wang, L., . . . Gao, J. (2015). Surface and Interfacial Engineering of Iron Oxide Nanoplates for Highly Efficient Magnetic Resonance Angiography. *ACS Nano*, *9*(3), 3012-3022. doi:10.1021/nn507193f

Zhu, N., Ji, H., Yu, P., Niu, J., Farooq, M. U., Akram, M. W., . . . Niu, X. (2018). Surface Modification of Magnetic Iron Oxide Nanoparticles. *Nanomaterials (Basel)*, *8*(10). doi:10.3390/nano8100810